Journal of Photochemistry and Photobiology, A: Chemistry, 53 (1990) 109 - 125

SOLUTE–SOLVENT RELAXATION OF ELECTRONICALLY EXCITED XANTHENE DYES

S. BERGAMASCO, G. CALZAFERRI† and K. HÄDENER

Institute for Inorganic and Physical Chemistry, University of Berne, Freiestrasse 3, CH-3000 Berne 9 (Switzerland)

(Received May 22, 1989)

Summary

Time-resolved fluorescence measurements were carried out on rhodamine 3B, pyronine B and rhodamine 101 ethylester in protic solvents of different viscosity but of similar dielectric properties by dual-beam multiple frequency phase fluorometry. Emission wavelength dependent biexponential fluorescence decay is reported for all combinations. The electronic nature of the xanthene skeleton with different N-substitution patterns was investigated as a function of the molecular conformation by semi-empirical calculations according to the extended Hückel molecular orbitals and the Pariser–Parr–Pople methods. No evidence in support of the twisted intramolecular charge transfer state model for the S_1 state is found in the correlation of experimental and computational results, but a qualitative interpretation for the viscosity dependence of the fluorescence quantum yields of dialkylamino-substituted xanthene dyes is given. The key factor determining the quantum yield was found to be the rigidity of the amino groups and their substitution pattern. The variation of the decay law with emission wavelength is discussed in terms of structural relaxation of the solute, dielectric relaxation of the solvent and specific solute–solvent interactions.

1. Introduction

The variability of organic dyes with regard to their luminescence behavior in diluted solutions can be attributed to a number of different processes. Of particular importance are specific intramolecular donor–acceptor interactions as well as the same type of interaction with the solvent, *e.g.* hydrogen bonding or acid–base reactions [1 - 5], and intramolecular charge redistribution inducing dielectric relaxation of the solvation shell [6 - 11]. Even though the net charge redistribution upon electronic excitation might

†Author to whom correspondence should be addressed.

1010-6030/90/$3.50

be small, it may substantially influence the luminescence behavior in combination with the rearrangement of solvent molecules and conformational changes of the solute. It is well established that fluorescence and phosphorescence quantum yields depend on the solute chromophore's rigidity and that solvent viscosity may dramatically affect the luminescence properties [12 - 18].

We have found that accurate fluorescence decay measurements of dyes such as rhodamine 6G, coumarine 535 and others reveal a significant emission wavelength dependent dual-exponential decay law, varying with the composition of the solvent [19 - 21]. Proof was given that this behavior is not caused by self-absorption and reemission [22]. In the case of rhodamine 6G we have speculated that the observed behavior could be due to different conformers stabilized by a viscous environment. Kinoshita *et al.* have pointed out that the experimental data available are not sufficient to distinguish between a mechanism based on the rearrangement of solvent molecules and between intramolecular large amplitude motions [23]. These authors assume that the fluorescence spectra of rhodamine 6G can be described by a single gaussian profile which in fact is a very poor approximation of the true lineshape. According to our experience, in ethanol the spectrum has to be simulated by three gaussians [24], while in glycerol a sum of two gaussians is sufficient.

In some recent papers on xanthene and related dyes, intramolecular donor–acceptor interaction (formation of biradicaloid charge-transfer states) involving amino group twisting was made responsible for the nonradiative deactivation [25, 26]. To elucidate to what extent this interpretation is consistent with our earlier observations [19 - 21] and to investigate the influence of intramolecular motion of the phenyl rest and of the amino groups on the particular luminescence kinetics, we have carried out precise fluorescence decay measurements for the structures in Scheme 1 as a function of the emission wavelength in solvents of different viscosity but of similar dielectric properties.

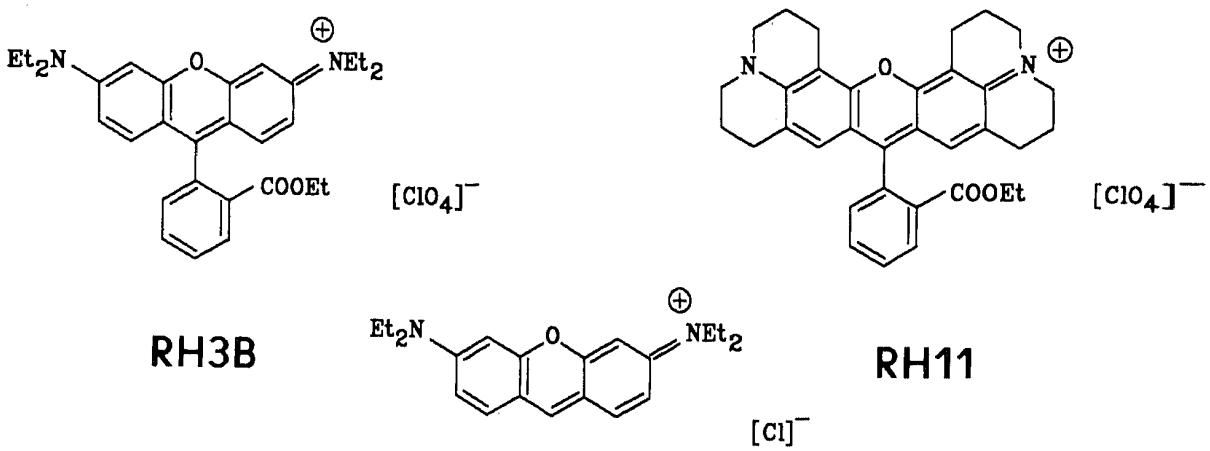

Scheme 1.

2. Experimental details

2.1. Dyes and solutions

Rhodamine 3B perchlorate (RH3B) and pyronine B chloride (PYRB) were obtained from Eastman Kodak Co. RH3B was lasergrade and used without further purification, and PYRB was purified by flash column chromatography on silica gel (Merck silica gel 60 for flash chromatography) applying gradient elution with acetone/methanol mixtures (2:1 up to 3:7), as proposed by Drake *et al.* [27]. Rhodamine 101 ethylester perchlorate (RH11) was obtained by esterification of rhodamine 101 (Eastman Kodak Co.) with sulfuric acid and ethanol. The reaction mixture was heated under reflux for 48 h, chilled and poured into an ice/water mixture. The precipitated solid was collected, dissolved in ethanol, and a small amount of 5% perchloric acid solution was added [28]. After chilling for 48 h, the solid ester perchlorate was collected. Thin layer chromatography analysis still showed small amounts of acid. Flash column chromatography on silica gel with chloroform/acetone (4:1) was therefore applied to obtain pure ester. ^{1}H-NMR spectra agree with the assigned structure. Glycerol (Merck, fluorescence microscopy grade) and water solutions of the dyes were made and then mixed to obtain solutions of 97, 50 and 10 mass percent glycerol. The concentration of each solution was 10^{-6} M within an error of approximately 1%, mixture effects included. The samples were degassed in standard 10-mm fused silica cells by a succession of three freeze–pump–thaw cycles and measured at the controlled temperature of 25 °C. Table 1 shows interpolated values for the viscosity η, the dielectric constant ϵ and the refractive index n for the three solvent mixtures at 25 °C [29 - 31].

2.2. Experimental set-up

The principle and instrumentation of the dual-beam multiple frequency phase fluorometry (MFPF) method has been described in previous articles [32 - 34]. An account of some important technical improvements leading to higher sensitivity and time resolution is given below.

TABLE 1

Physical solvent properties at 25 °C

Composition (mass-% glycerol)	*Viscosity*[a] (cP)	*Dielectric constant*[b]	*Refractive index*[c]
97	500	50	1.470
50	5	66	1.394
10	1.2	75	1.345

[a] From ref. 29.
[b] From ref. 30.
[c] From ref. 31.

Figure 1 shows the current set-up. The light source is a krypton ion CW laser (Spectra Physics Mod. 171-01) operating with single line option. Its beam is first modulated by an acousto-optic modulator (Intra Action 403) with a constant frequency of 1700 Hz and by an electro-optic modulator (EOM, Conoptics 380) in the frequency range from 5 to 200 MHz. A Coherent Associates 3050 EOM system can be installed to cover the low frequency range. The ordinary beam of the EOM is reflected by a corner cube mounted on a translation stage, which can be positioned motor driven with an accuracy of 0.1 mm over a length of 150 cm. The beam then passes through a polarization rotator and hits the reference cell after having been attenuated by two Glan prisms. The extraordinary beam of the EOM with a mean power of less than 30 mW is used for fluorescence excitation and may be delayed to optimize the phase relation to the ordinary beam. The scattered light of the reference (colloidal SiO_2, 0.32% LUDOX HS (DuPont) in water) is focused into a bundle of quartz fibers, while the luminescence of the sample is first wavelength selected by a monochromator with a 4-nm bandwidth (Jobin Yvon HD10). For decay measurements, magic angle polarizers are inserted into the focusing system. The optical fibers of reference and sample are mixed randomly to give the same image on the photomultiplier tube (PMT, Hamamatsu R928). The signal of the cooled and r.f.

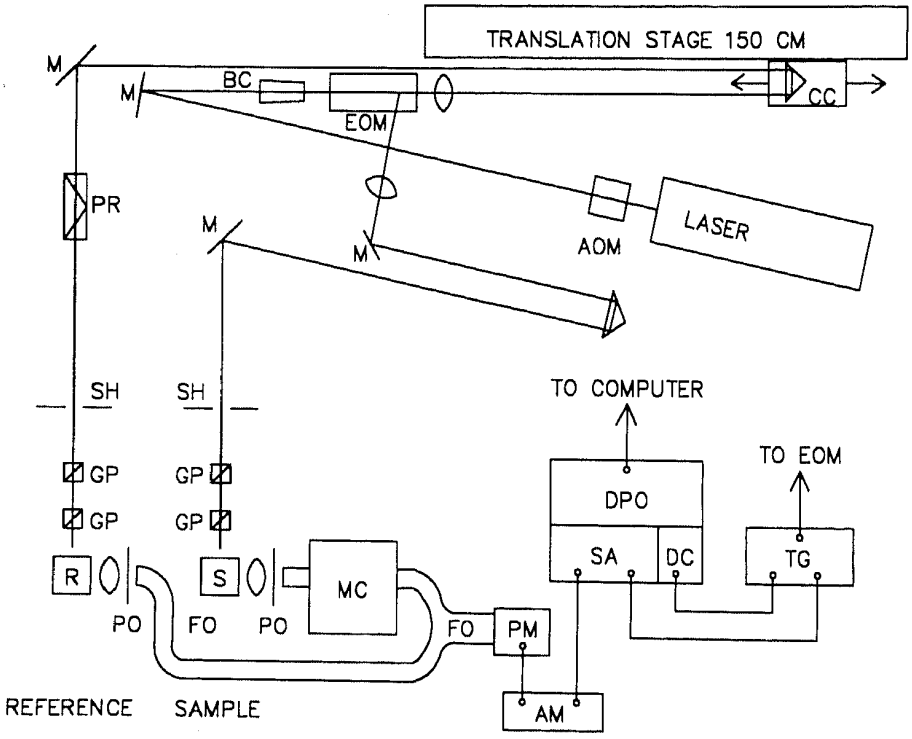

Fig. 1. Experimental set-up of the dual-beam MFPF fluorometer. AOM, acousto-optic modulator; M, mirror; BC, beam collimator; EOM, electro-optic modulator; CC, corner cube; PR, polarization rotator; SH, shutter; GP, Glan prism; R, reference cell; S, sample cell; PO, sheet polarizer; FO, fibre optic; MC, monochromator; PM, photomultiplier; AM, amplifier; SA, spectrum analyzer; DPO, digital processing oscilloscope; DC, digital counter; TG, tracking generator.

shielded PMT is converted and amplified [34] and detected by a spectrum analyzer (Tektronix 7L13) with a bandwidth of 30 Hz; the analyzer's local oscillators are coupled to a tracking generator (Tektronix TR501) that drives the EOM through a h.f. broadband amplifier (ENI 550L). A digital processing oscilloscope (Tektronix P7701) transmits acquired waveforms to the controller of the experiment (DEC PDP-11/23) for data reduction.

2.3. Data analysis

The measured phase differences ϕ as a function of the circular modulation frequency ω are modelled by a multiexponential decay function [19]:

$$\tan \phi(\omega) = \omega \left[\sum_{i=1}^{n} \frac{\alpha_i \tau_i}{1 + \omega^2 \tau_i^2} \right]^{-1} \sum_{i=1}^{n} \frac{\alpha_i \tau_i^2}{1 + \omega^2 \tau_i^2} \tag{1}$$

corresponding to an impulse response T in the time domain [20, 21]:

$$T(t) = \left[\sum_{i=1}^{n} \alpha_i \tau_i \right]^{-1} \sum_{i=1}^{n} \alpha_i e^{-t/\tau_i} \tag{2}$$

The parameters α_i and τ_i are estimated in a weighted non-linear least-squares fit using procedure NLIN of the statistical analysis system SAS [35], with $\alpha_1 \equiv 1.0$ for normalization. The minimized entity is $\chi_r^2 = \chi^2/\nu$, where ν denotes the number of degrees of freedom [36]. Each fit is regularly repeated with the vertices of a $(2n-1)$-dimensional grid as varying starting points, and the quality is judged on the basis of the final χ_r^2, the distribution of the residuals and the correlation matrix.

3. Results

3.1. Measurements

Glycerol/water solutions (97%, 50% and 10%) of the dyes RH3B, PYRB and RH11 were measured at ten equidistant modulation frequencies in the range of 30 to 138 MHz, excited at the krypton laser line of 530.9 nm (less than or equal to 10 mW). The optical path was 5 mm since 1 cm cells were used in a right angle detection geometry. The results of the corresponding fits are summarized in Table 2.

In general the minimum number of exponential terms necessary to describe the decay behavior is two for all three dyes; as an exception, three terms are used at the emission wavelengths of 640 and 655 nm for RH3B, and 655 and 670 nm for PYRB, respectively. In these cases, because of a high degree of correlation among the parameters, τ_3 was fixed at the value indicated in the table, which proved generally acceptable for all four cases. The relative weights α_2 of the lifetime τ_2 and to a lesser extent also τ_1 are pronounced functions of the emission wavelength (Fig. 2, Table 2).

TABLE 2

Fluorescence decay parameters at 25 °C

C^a	λ^b	*Rhodamine 3B* (1.00×10^{-6} M)					*Pyronine B* (1.00×10^{-6} M)					*Rhodamine 101-EE* (1.02×10^{-6} M)				
		τ_1[c]	2σ	α_2	2σ	χ_r^2	τ_1[d]	2σ	α_2	2σ	χ_r^2	τ_1[e]	2σ	α_2	2σ	χ_r^2
97%	550	3.430	0.049	1.307	0.045	1.87	3.357	0.039	1.059	0.026	2.66					
	565	3.321	0.011	0.680	0.007	0.49	3.276	0.017	0.342	0.009	0.48	3.283	0.066	0.761	0.062	1.93
	580	3.253	0.017	0.132	0.007	0.59	3.390	0.019	−0.051	0.007	0.91	3.505	0.056	0.544	0.040	4.07
	595	3.357	0.014	−0.095	0.005	0.50	3.501	0.020	−0.170	0.007	1.10	3.663	0.054	0.225	0.028	2.21
	610	3.356	0.048	−0.187	0.016	3.88	3.478	0.014	−0.138	0.005	0.24	3.818	0.022	−0.041	0.008	0.44
	625	3.406	0.017	−0.070	0.007	0.64	3.476	0.012	−0.083	0.006	0.31	3.972	0.060	−0.123	0.032	3.02
	640	3.450[f]	0.000	0.296	0.079	2.59	3.489	0.018	−0.173	0.007	0.33	3.919	0.040	−0.078	0.026	1.80
	655	3.450[g]	0.000	0.013	0.058	0.95	3.480[h]	0.000	−0.202	0.084	1.35	3.886	0.060	−0.004	0.026	1.53
	670	3.448	0.047	−0.214	0.019	1.79	3.570[i]	0.000	−0.182	0.036	0.20	3.925	0.048	−0.025	0.018	0.91
	685	3.439	0.001	−0.198	0.001	3.70	3.556	0.013	−0.144	0.006	0.07	3.987	0.032	−0.038	0.026	0.45
	700											4.001	0.166	0.060	0.152	1.25
50%	550	2.564	0.024	1.024	0.030	0.94	2.642	0.015	1.062	0.019	0.41					
	565	2.409	0.026	0.665	0.036	3.08	2.556	0.017	0.544	0.017	1.09	4.105	0.090	0.357	0.068	0.42
	580	2.392	0.019	0.528	0.019	1.26	2.603	0.015	0.398	0.012	0.81	4.119	0.052	0.165	0.024	1.33
	595	2.323	0.015	0.402	0.016	3.01	2.584	0.022	0.345	0.018	1.64	4.138	0.030	0.043	0.012	0.72
	610	2.374	0.017	0.447	0.017	0.95	2.572	0.021	0.377	0.019	1.83	4.121	0.070	−0.031	0.022	4.26
	625	2.361	0.012	0.468	0.015	0.55	2.597	0.024	0.441	0.024	1.16	4.099	0.064	−0.061	0.022	2.96
	640	2.360	0.012	0.477	0.017	1.29	2.616	0.022	0.413	0.021	1.93	4.186	0.028	−0.018	0.005	0.32
	655	2.407	0.018	0.511	0.021	0.95	2.625	0.018	0.407	0.017	1.61	4.169	0.018	−0.003	0.010	0.35
	670	2.398	0.020	0.484	0.023	1.32	2.655	0.018	0.449	0.020	0.91	4.410	0.120	−0.010	0.046	7.45
	685	2.396	0.014	0.481	0.020	0.70	2.625	0.032	0.449	0.035	2.54	4.184	0.076	−0.028	0.034	1.32
	700											4.134	0.048	−0.071	0.026	0.35
10%	550	2.123	0.039	1.064	0.082	1.50	2.138	0.082	1.362	0.167	4.69					
	565	1.671	0.028	1.155	0.047	2.36	1.798	0.022	0.194	0.035	5.67	3.832	0.052	0.191	0.022	0.36
	580	1.613	0.029	−0.033	0.047	2.76	1.830	0.046	0.076	0.063	5.84	4.164	0.148	0.156	0.048	4.72
	595	1.665	0.036	0.034	0.057	3.72	1.780	0.050	−0.005	0.007	5.78	4.178	0.056	0.044	0.018	0.81
	610	1.652	0.024	0.017	0.039	1.80	1.783	0.023	0.025	0.029	3.66	4.170	0.058	0.009	0.018	1.28
	625	1.703	0.017	0.109	0.027	1.13	1.787	0.027	0.029	0.036	1.83	4.373	0.164	0.090	0.044	5.76
	640	1.644	0.019	0.010	0.029	1.34	1.881	0.037	0.137	0.055	5.86	4.233	0.148	0.072	0.044	5.09
	655	1.728	0.031	0.129	0.049	1.20	1.866	0.036	0.067	0.046	3.50	4.274	0.084	0.116	0.046	2.31
	670	1.688	0.031	0.049	0.050	0.96	1.859	0.041	0.075	0.058	1.12	4.207	0.096	0.050	0.032	0.95
	685	1.732	0.047	0.114	0.084	1.26	1.903	0.074	0.157	0.097	1.70	4.258	0.084	0.085	0.034	0.44

[a] Mass percent of glycerol.
[b] Detection wavelength (nm).
[c] Nanoseconds, $\alpha_1 = 1.0$; $\tau_2 = 0.85$ ns; $\pm 2\sigma$: 95% confidence interval.
[d] Nanoseconds, $\alpha_1 = 1.0$; $\tau_2 = 0.85$ ns.
[e] Nanoseconds, $\alpha_1 = 1.0$; $\tau_2 = 0.85$ ns.
[f] $\tau_3 = 75$ ps; $\alpha_3 = -2.493 \pm 0.519$.
[g] $\tau_3 = 75$ ps; $\alpha_3 = -1.127 \pm 0.418$.
[h] $\tau_3 = 75$ ps; $\alpha_3 = -3.340 \pm 0.614$.
[i] $\tau_3 = 75$ ps; $\alpha_3 = -1.446 \pm 0.258$.

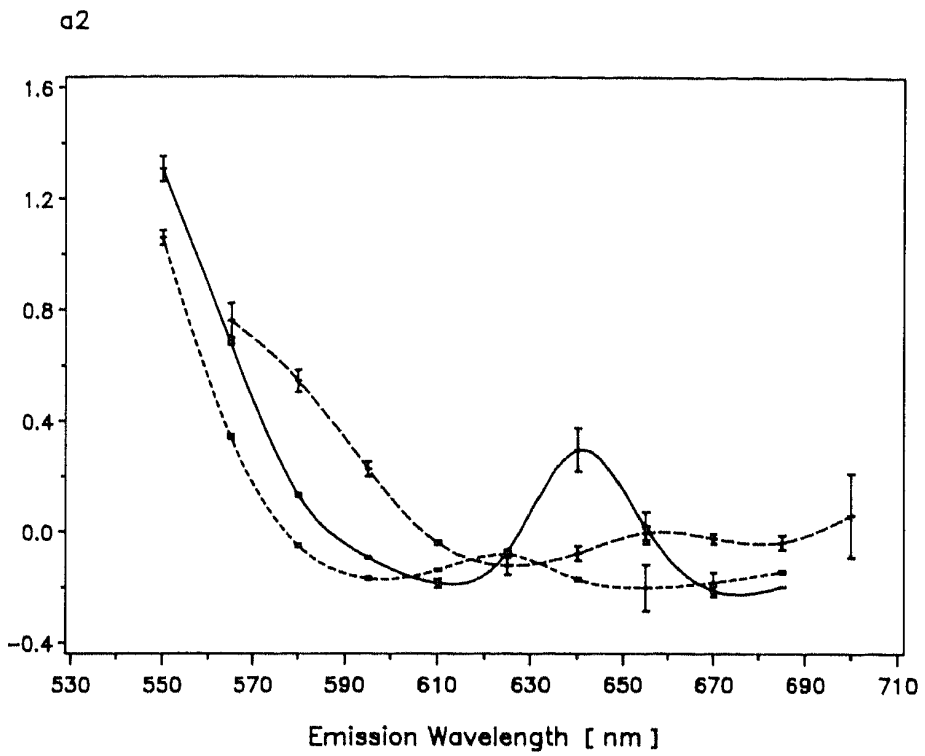

Fig. 2. Relative weights α_2 of the lifetime τ_2. Dyes (10^{-6} M in 97% glycerol/water, 25 °C): —— rhodamine 3B; - - - - pyronine B; — — — rhodamine 101-EE; error bars indicate 95% confidence intervals.

Common to all three structures, RH3B, PYRB and RH11, independent of solvent composition, is a sharp drop in the value of α_2 within the high energy spectral region. While for the high viscosity solutions this decrease takes place within the lowest 50 nm of the emission spectrum interval covered by measurements, in the 10% glycerol solution it is much steeper with α_2 approaching zero within about 25 nm. Disregarding the local maxima present in the central parts of all graphs in Fig. 2, a general transition to a nearly mono-exponential decay law in the red tail of the spectrum becomes apparent. For the 97% glycerol solutions α_2 is relatively small in this part of the spectrum, but still significantly negative, whereas at the 10% concentration it is significantly positive. In the 50% solvent mixture RH3B and PYRB show an α_2 plateau at around 0.45, while with RH11 this parameter becomes slightly smaller than zero in the red region; the emission spectrum and the associated characteristic of the decay parameters are red-shifted for RH11 relative to the other dyes by about 25 nm.

With regard to τ_1 as a function of emission wavelength and solvent composition (Fig. 3) the three dyes can be classified into two groups. RH3B and PYRB show strong solvent dependence in that their τ_1 values drop in parallel to their fluorescence quantum yields η_i with increasing water content of the solvent, *i.e.* the η_i are 0.48, 0.35 and 0.27 (RH3B), and 0.53, 0.48 and 0.39 (PYRB) for the compositions 97%, 50% and 10%, respectively. The primary fluorescence lifetime, if we shall give τ_1 this label, and the quantum yield of 0.3 of RH11 on the other hand are to a large extent unaffected by the varying solvent properties.

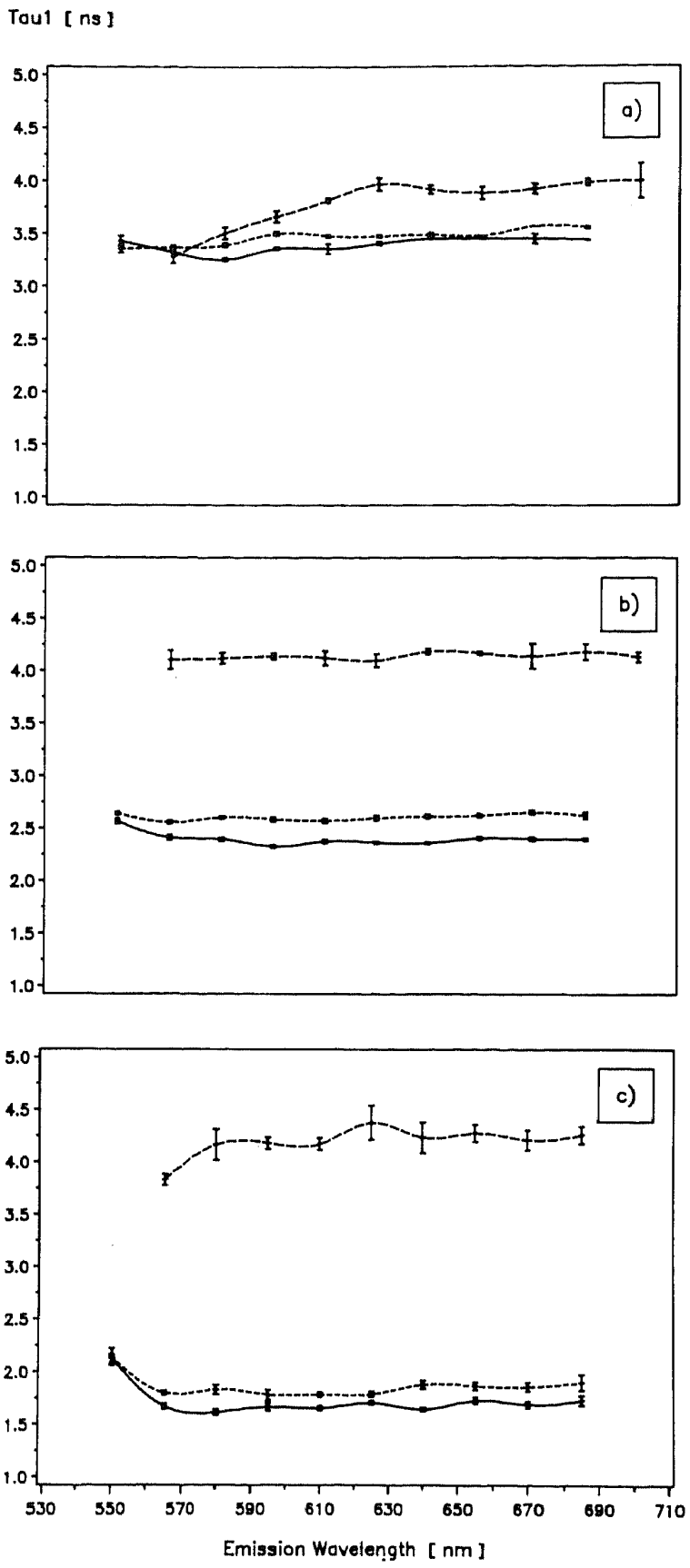

Fig. 3. Lifetimes τ_1 as a function of solvent composition. Dyes (10^{-6} M, 25 °C): —— rhodamine 3B; - - - - pyronine B; — — — rhodamine 101-EE; error bars indicate 95% confidence intervals. (a) 97% Glycerol/water; (b) 50% glycerol/water; (c) 10% glycerol/water.

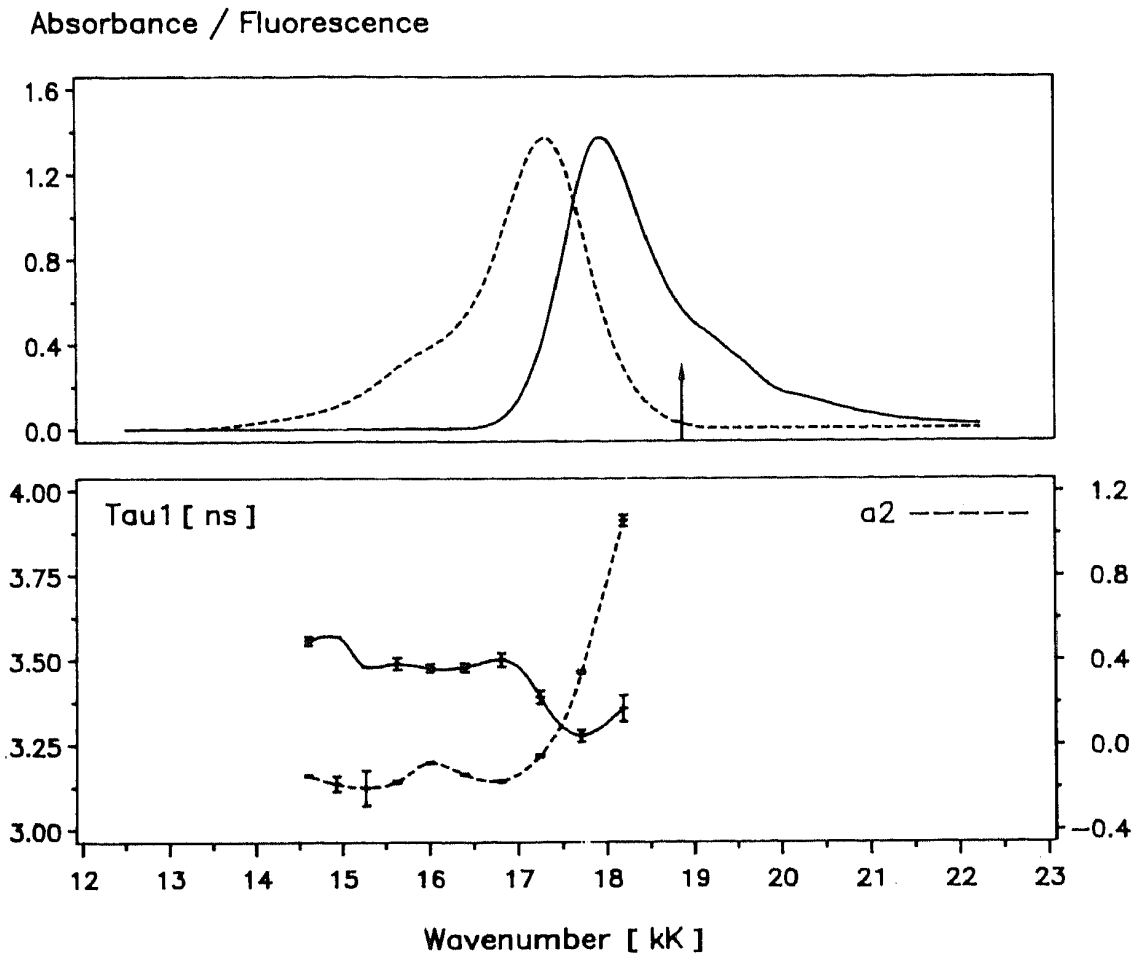

Fig. 4. Absorption/fluorescence spectrum of pyronine B (10^{-6} M in 97% glycerol/water, 25 °C). Upper part: corrected fluorescence intensity - - - - normalized to equal maxima; lower part: decay parameters with 95% confidence intervals (τ_2 = 850 ps).

The absorption and emission spectra of the three dyes in the solvents considered show general mirror symmetry as demonstrated for PYRB in Fig. 4. Although the spectra overlap considerably, fluorescence reabsorption has been shown to be negligible in the concentration–path length regime applied [22]. The 530.9 nm excitation line is indicated in this figure by an arrow. The significant spectral variation of τ_1, suppressed in the other representations, is very evident from Fig. 4. The shoulders found at a distance of 1400 cm^{-1} from the spectral maxima are present in all the spectra and can be attributed to a number of aromatic C–C stretching vibrations [37].

A hypsochromic solvent shift of about 200 cm^{-1} is apparent from Fig. 5, comparing the absorption spectra of the 97% and 10% glycerol solutions, while the emission spectra are practically unaffected.

3.2. Molecular orbital calculations

To support the interpretation of the experimental results, molecular orbital calculations on the basis of the Pariser–Parr–Pople (PPP) [38] and the extended Hückel molecular orbitals (EHMO) method [39] were performed.

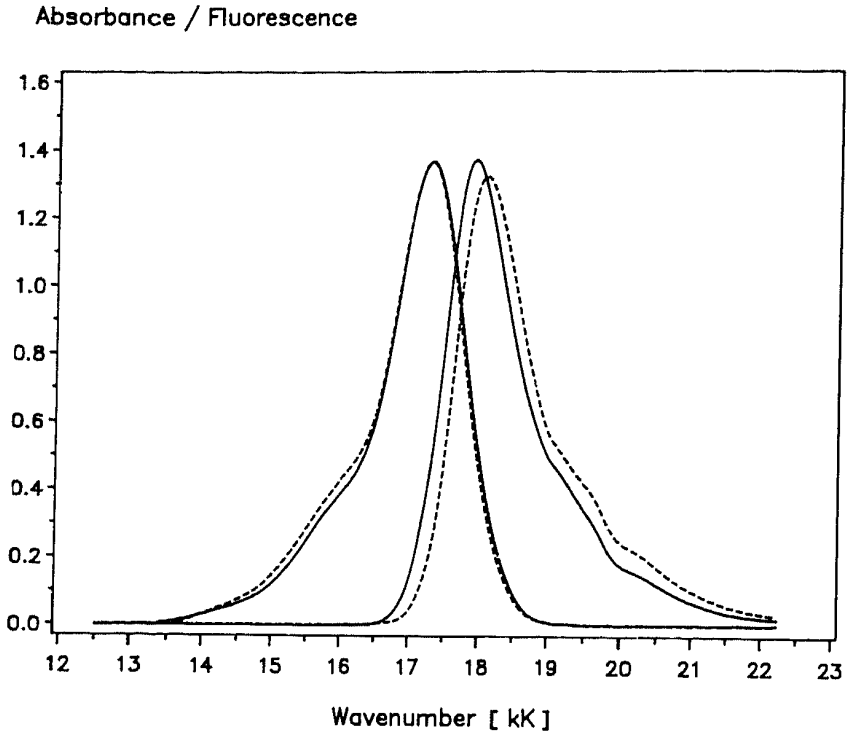

Fig. 5. Solvent dependence of pyronine B spectra. Pyronine B (10^{-6} M) absorption and emission spectra at 25 °C: —— in 97% glycerol/water; - - - - in 10% glycerol/water. Corrected fluorescence intensity normalized to equal maxima; excitation at 530.9 nm.

The main result of the PPP–CI calculation is the finding that a single configuration is adequate and sufficient for the description of the S_0 and S_1 state in the planar forms of the dyes. For this reason and because in non-planar geometries σ–π interactions become important we will restrict our discussion to the EHMO results. Table 3 lists the parameter set used for the extended Hückel calculations, and Table 4 describes the planar input geometries in terms of bond lengths and angles.

Since the grouping of the dyes mentioned in the previous section suggests a dominant role for the dialkyl amino groups' mobility, a series of EHMO calculations with varying torsion angles of these groups was performed; the amino groups themselves were kept planar during this

TABLE 3

EHMO parameters[a]

Atom	*S*			*P*		
	N	*Exp*	*Coul* (eV)	*N*	*Exp*	*Coul* (eV)
H	1	1.300	−13.60			
C	2	1.625	−21.40	2	1.625	−11.40
N	2	1.950	−26.00	2	1.950	−13.40
O	2	2.275	−32.30	2	2.275	−14.80

[a]Hückel constant $K = 1.75$.

TABLE 4

EHMO input geometries

	Center			*Value*	*Comment*
Bond length (Å)	C	C		1.400	
	C	O		1.400	
	C	H		1.060	Aromatic C
	C	H		1.090	Methyl group
	C	N		1.470	Aromatic C, N
	N	C		1.479	
	N	H		1.034	
Bond angle (degrees)	C	C	C	120.0	
	C	O	C	120.0	
	C	C	N	120.0	
	C	N	C	120.0	One H of each $-CH_3$ group
	H	C	H	109.3	in the molecular plane
	H	N	H	120.0	towards center

process, *i.e.* no pyramidalization of the nitrogen atoms was introduced. The influence of the amino substitution pattern was investigated for the $-NH_2$, $-NH(CH_3)$ and $-N(CH_3)_2$ symmetrically substituted dyes; the methyl group instead of the ethyl substituent was used to reduce the computational burden and conformational degrees of freedom. Both amino groups were rotated synchronously, maintaining maximum molecular symmetry. The resulting homo and lumo charge distributions extracted from the reduced charge matrix as a result of the Mulliken population analysis [40] for the 0° (planar) and 90° torsional angle conformations are shown in Scheme 2. In this representation use is made of the charge

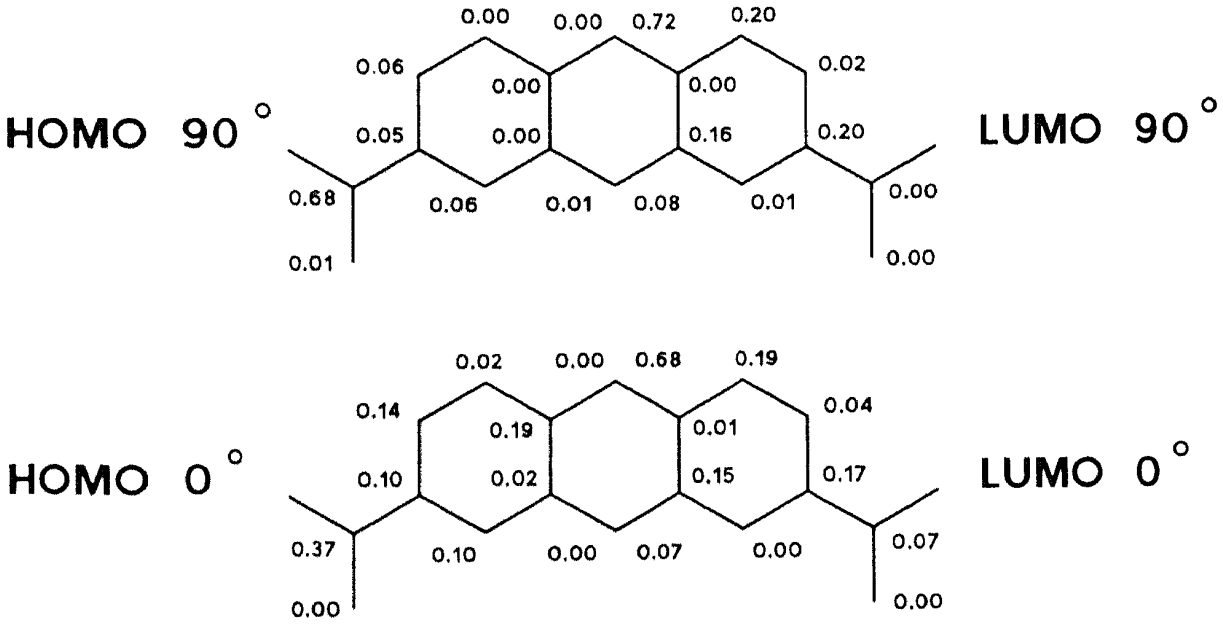

Scheme 2.

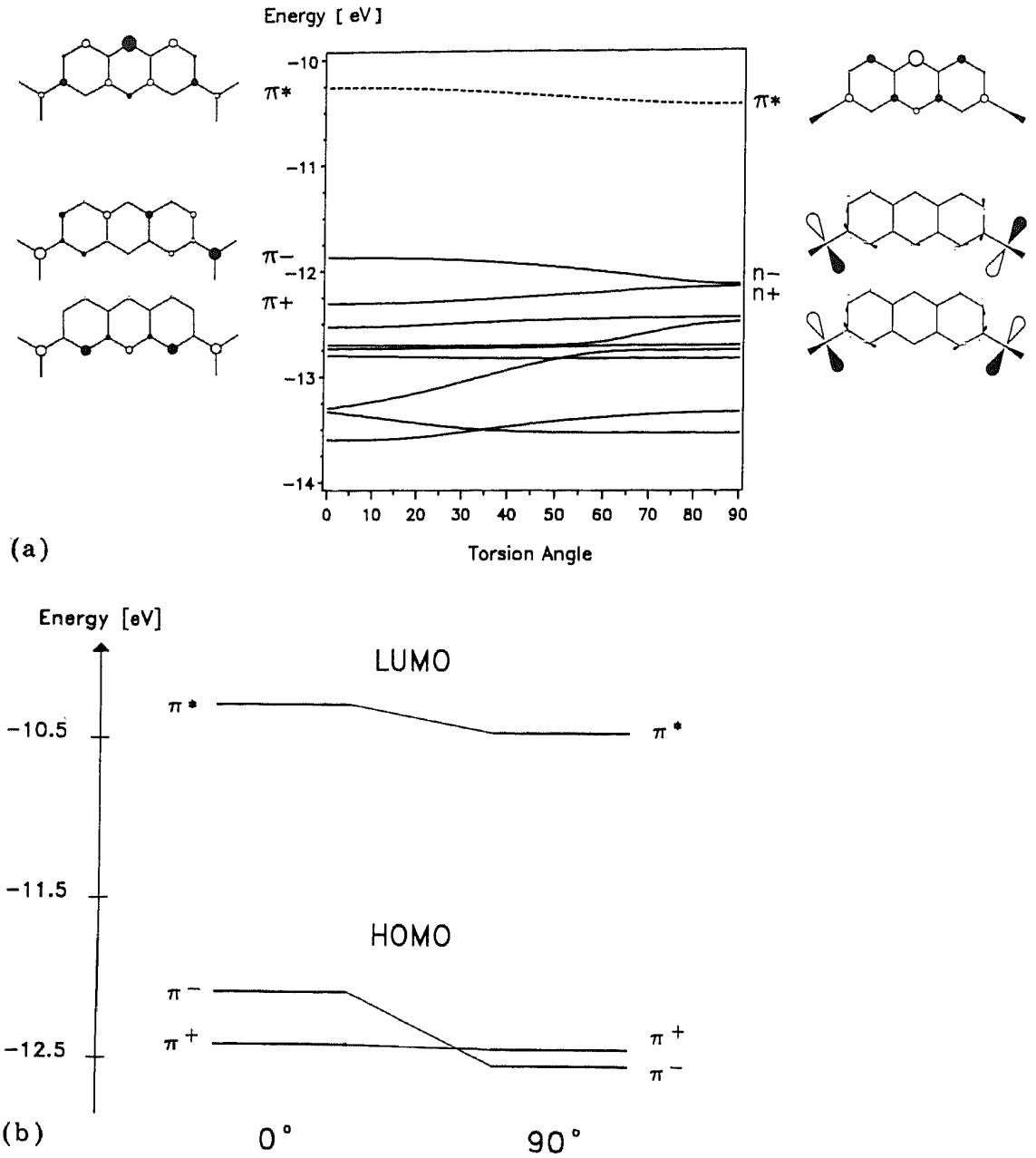

Fig. 6. MO correlation diagram for planar and 90° conformations. (a) Pyronine B, both amino groups $-N(CH_3)_2$ substituted: MO energy and coefficients as a function of amino group torsion angle; (b) correlation for unsubstituted amino groups.

distribution's mirror symmetry in that the matrix elements for *homo* and *lumo* are depicted on the two halves of the same structure skeleton. Basically negative charge is transferred upon excitation from the amino nitrogen atoms to the carbon atom in the nine-position to about the same extent in both conformations. The corresponding change in dipole moment is relatively small, since for symmetry reasons only the charge transfer component parallel to the short molecular axis is relevant.

The frontier orbitals for the planar and twisted conformations are shown in the correlation diagram in Fig. 6(a), while Fig. 6(b) is a comparison with the $-NH_2$ substituted structures. The correlation of the *homo*π-

and n-type orbitals in Fig. 6(a) may appear unusual at first sight but has its explanation in the fact that the classification criterion, the σ_h symmetry plane, is not preserved along the rotation coordinate serving as the ordinate in this diagram.

4. Discussion

One of the main goals of this work was the investigation of the role played by the mobility of the different substituents to the same basic xanthene structure. In previous publications [19] we had speculated that viscous rotation of the phenyl ring in rhodamine 6G as well as RH3B and RH11 might be responsible for the observed viscosity dependence of the fluorescence quantum yield and decay parameters. In the light of the results given in the present study it seems safe to say that the influence of this substituent on the luminescence properties of the dye is of secondary importance. The key factor determining the quantum yield is decidedly the rigidity of the amino groups and their substitution pattern.

Although a dual exponential fluorescence decay law for this class of dyes in low viscosity solvents such as ethanol at room temperature was not confirmed by other authors [25], we have found it to be the general case for the dyes investigated in this work and a number of laser dyes studied earlier [21]. The suggestion prominent from Fig. 2 is that the parameters of the phenomenological decay law are pronounced functions of the emission wavelength and consequently that they should only be discussed in their dependence on the corresponding fluorescence wavelengths. As shown in ref. 19, this kind of relation of decay law and emission spectrum is compatible with the conjecture of more than one emitting state, and the observed α_2 characteristic can be explained by the assumption of a second, energetically relaxed, excited state that is populated through the first one. The nature of the process leading to this excited state relaxation shall be the matter of the following discussion.

Vogel *et al.* have recently reported a fluorescence spectroscopic study of rhodamine dyes very similar to the ones investigated in this work with different N-substitution patterns [25]. They interpret the viscosity dependence of their decay data as a result of structural relaxation of the amino groups allowing the formation of a non-emissive twisted intramolecular charge-transfer (TICT)-like state with charge localization. This TICT state formation is claimed to be possible only for dialkylamino substituted dyes.

Our molecular orbitals calculations do indeed predict a different behavior of the S_1 state for the $(-NH_2)_2$ and $(-N(CH_3)_2)_2$ case as shown in Fig. 6. The orbital type in the *homo* region as a function of torsion angle in the $-NH_2$ case was found to be somewhat susceptible to the value of the Hückel constant and torsion coordinate used, but this finding does not affect the essence of the following accounts. While in the structure with free $-NH_2$ groups the first excited singlet state is of π–π^* symmetry independent of the amino groups' rotational angle, this state acquires n–π^*-symmetry in the 90°

conformation of the dimethylamino substituted structure. In this conformation the optical transition is formally forbidden; the transition moment μ for the intermediate rotation angles ϕ is estimated on the basis of the ZDO approach:

$$\mu(\phi) \propto \left[\sum_i (c_i^{\mathrm{LUMO}}(\phi) \cdot x_i \cdot c_i^{\mathrm{HOMO}}(\phi)) \right]^2 \qquad (3)$$

where c_i are the coefficients of the p_z orbitals in the corresponding MO and x_i represents the unit length x-component of the center i coordinates. $\mu(\phi)$ is plotted in Fig. 7; up to a rotation angle of about 20° it is almost constant and decreases linearly with increasing angle after that. Assuming a nearly planar ground state conformation the Franck–Condon geometry of an excited dye molecule will also be planar. If the rotation of the amino groups in this excited state is energetically feasible and allowed, by the microviscosity of the surrounding solvent, to occur on a time scale comparable with the lifetime of this state, then a dramatic reduction in fluorescence quantum yield for the dialkylamino case would be expected, while in the structure with unsubstituted amino groups the quantum yield should be independent of amino group mobility. This idea implies a finite non-radiative decay rate which should be comparable in both cases and work in concurrence to the radiative processes.

The ground state torsion potentials furnished by the EHMO calculations yield an interesting picture of the amino group mobility in the different structures studied, and we do not expect the S_1 potentials to have a significantly different characteristic, above all since equal π bond orders are

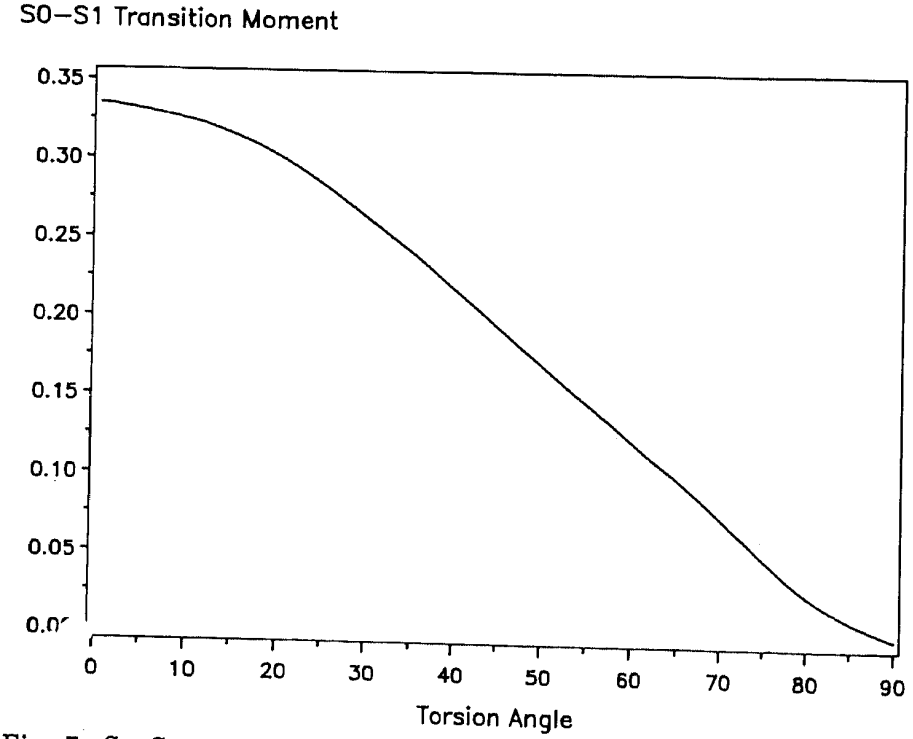

Fig. 7. S_0–S_1 transition moment in ZDO approximation. Transition moment μ as a function of amino group torsion angle ϕ (eqn. (3)).

found for the C—NH_2 bond in the S_0 and S_1 state by the PPP–CI method (ten configurations). While for the carbon-amino and -methylamino bonds the calculations yield a rotation barrier of the order of 0.8 eV, a rotation potential with a shallow minimum in a slightly twisted geometry is predicted for the dimethylamino substituent. If from this finding the conclusion is drawn that at room temperature rotation of the amino groups is possible only if they are dialkylated, then agreement is attained with the results of Vogel *et al.* [25] reporting temperature independent fluorescence quantum yields close to unity for the amino and monoalkylamino substituted xanthene dyes in contrast to highly temperature dependent quantum yields for the dyes with dialkylamino groups. With RH11 the amino groups have essentially no degrees of rotational freedom independent of solvent composition and temperature, and as evident from Fig. 3, this dye's radiative lifetime is consequently independent of solvent viscosity. Considering the charge redistribution in the symmetrically dimethylamino substituted pyronine (Scheme 2) as a function of twist angle, a minimum of stabilization of the 90°-conformation over the planar one even in highly polar solvents is to be expected; the extent of charge transfer from the nitrogen atoms to the carbon atom in the nine-position is only slightly larger for the twisted excited state. The necessity of a TICT state formation is not very obvious under this viewpoint. Although in any case the amount of transferred electronic charge is considerable, the overall change in dipole moment is very moderate because its components along the principal molecular axis cancel. The two diagonal components along the N—C(9) distances (5.7 Å), however, are large, change sign upon excitation and in polar solvents should thus induce a local reorientational relaxation of the innermost solvent shells. This sort of dielectric relaxation could explain the 0.85 ns lifetime and its spectral dependence found in the phenomenological decay law of the rhodamines under study. The spectral shift correlation function $C(t)$, however, which is normally used to describe the temporal evolution of the emission spectrum [11], should then be defined in an adequate manner. The characteristic frequency $\tilde{\nu}_f(t)$ usually describes the emission maximum shifting with time as the solvent relaxes; the wavelength dependent decay laws found for the three dyes in Scheme 1, however, do not correspond to a general shift of a fluorescence peak but rather to a build-up of emission intensity in the red tail of the spectrum. Hence, the maximum of the time dependent emission spectrum generated based on the assumptions described in ref. 24 does not shift, and for a quantitative treatment of the spectral redistribution of intensity the weighted mean fluorescence frequency, for example, could be used as $\tilde{\nu}_f(t)$. Facing the differences between the traditional point dipole concept of a solute particle and the realistic charge distributions discussed above within our dye molecules, and considering the apparent importance of solute conformational changes for the excited state relaxation as well as the present lack of applicable theories of molecular aspects of solvation, we do not attempt a quantitative interpretation of the solvent dependence of our time resolved fluorescence data yet. The demands

made upon such a treatment would not only include an explanation for the observed $\alpha_2(\tilde{\lambda})$ characteristic but also for the significant wavelength dependence of τ_1. We do not expect the current dielectric continuum theories of the solvent to succeed in resolving these subtleties.

Another potential source of interference with radiative relaxation of excited dye molecules in solution so far excluded from the discussion are specific solute–solvent interactions. Taking into account the steady state spectra of Fig. 5, where invariance of the emission spectrum of PYRB with solvent polarity is observed, the existence of a highly stabilized (twisted) charge transfer state with charge localization is again not plausible. Altogether unexplained by such a hypothesis is the empirical blue shift of the absorption spectrum with increasing water content of the solvent. Baba *et al.* have observed similar shifts in the $n \rightarrow \pi^*$ absorption spectra of several diazines in solvents of varying hydrogen bond donating potential and have interpreted the positive correlation between the hypsochromic shift of the absorption maximum and the "proticity" of the solvent as an indication of increasing S_0 state stabilization by intermolecular hydrogen bonds [41]. The interaction of protic solvent molecules with the dimethylamino group of 4-(*N*,*N*-dimethylamino)benzonitrile (DMABN) has recently gained much interest and has been investigated by several groups in molecular beam experiments [42, 43] and in solution [44]. From our results and the findings of these studies we conclude that specific interactions of the dye cations with solvent molecules, in particular involving the lone electron pairs of the amino nitrogens as acceptors, are important for the stabilization of the probe molecule. Especially the twisted conformation of the dialkylamino-substituted xanthenes in the S_0 state should therefore be susceptible to this form of interaction, and a shift of the ground state torsion potential minimum to a larger twist angle would be expected. As shown above, a reduction in oscillator strength would have to result from such a change in average geometry, and exactly this effect is evident from Fig. 5.

Acknowledgments

This work was supported by grant No. 2-5.542 of the Swiss National Science Foundation. We would like to thank R. Bühler for his continued help in dye purification and sample preparation.

References

1 A. Weller, in G. Porter (ed.), *Progress in Reaction Kinetics*, Vol. 1, Pergamon, Oxford, 1961, p. 189.
2 T. Förster and S. Völker, *Z. Phys. Chem. NF, 97* (1975) 79.
3 M. Itoh, T. Adachi and K. Tokumura, *J. Am. Chem. Soc., 106* (1984) 850.
4 E. Bardez, E. Monnier and B. Valeur, *J. Phys. Chem., 89* (1985) 5031.
5 F. A. Burkhalter, E. E. Meister and U. P. Wild, *J. Phys. Chem., 91* (1987) 3228.
6 E. Lippert, *Z. Elektrochem., 61* (1957) 962.

7 Z. R. Grabowski, K. Rotkiewicz, W. Rubazawska and E. Kiskor-Kaminska, *Acta Phys. Pol. A, 54* (1978) 767.
8 R. B. Macgregor, Jr. and G. Weber, *Ann. N.Y. Acad. Sci., 366* (1981) 140.
9 E. M. Kosower, *Acc. Chem. Res., 15* (1982) 259.
10 W. Rettig and R. Gleiter, *J. Phys. Chem., 89* (1985) 4676.
11 M. Maroncelli and G. R. Fleming, *J. Chem. Phys., 86* (1987) 6221.
12 G. Oster and Y. Nishiyima, *Fortschr. Hochpolym. Forsch., 3* (1964) 331.
13 D. Gegiou, K. A. Muszkat and E. Fischer, *J. Am. Chem. Soc., 90* (1968) 3907.
14 S. Sharafy and K. A. Muszkat, *J. Am. Chem. Soc., 93* (1971) 4119.
15 T. Förster and G. Hoffmann, *Z. Phys. Chem. NF, 75* (1971) 63.
16 G. Calzaferri, H. Gugger and S. Leutwyler, *Helv. Chim. Acta, 59* (1976) 1969.
17 J. Jansen and W. Lüttke, *J. Mol. Struct., 81* (1982) 207.
18 H. Güsten and R. Meisner, *J. Photochem., 21* (1983) 53.
19 J. Baumann, G. Calzaferri, L. Forss and T. Hugentobler, *J. Photochem., 28* (1985) 457.
20 J. Baumann, *Ph.D. Thesis*, Inst. Inorg. and Phys. Chem., University of Berne, Freiestrasse 3, CH-3000 Berne, 1984.
21 T. Hugentobler, *Ph.D. Thesis*, Inst. Inorg. and Phys. Chem., University of Berne, Freiestrasse 3, CH-3000 Berne, 1987.
22 J. Baumann, G. Calzaferri and T. Hugentobler, *Chem. Phys. Lett., 116* (1985) 66.
23 S. Kinoshita, N. Nishi and T. Kushida, *Chem. Phys. Lett., 134* (1987) 605.
24 G. Calzaferri and T. Hugentobler, *Chem. Phys. Lett., 121* (1985) 147.
25 M. Vogel, W. Rettig, R. Sens and K. H. Drexhage, *Chem. Phys. Lett., 147* (1988) 452 and 461.
26 M. Vogel, W. Rettig, U. Fiedeldei and H. Baumgärtel, *Chem. Phys. Lett., 148* (1988) 347.
27 J. M. Drake, R. I. Morse, R. N. Steppel and D. Young, *Chem. Phys. Lett., 35* (1975) 181.
28 G. A. Reynolds, *U.S. Patent 3932415*, 1976.
29 *Landolt Börnstein*, 6th Edn. Vol. II 5a, Springer, Berlin, 1959, p. 317.
30 *Landolt Börnstein*, 6th Edn. Vol. II 6, Springer, Berlin, 1959, p. 751.
31 *CRC Handbook of Chemistry and Physics*, 62nd edn., 1981, p. D-210.
32 H. Gugger and G. Calzaferri, *J. Photochem., 13* (1980) 21.
33 J. Baumann and G. Calzaferri, *J. Photochem., 23* (1983) 387.
34 K. Hädener, S. Bergamasco and G. Calzaferri, *Rev. Sci. Instrum., 59* (1988) 1924.
35 SAS Institute Inc., *SAS User's Guide: Statistics*, 5th Edn., SAS, Cary, NC, 1985, p. 575.
36 P. R. Bevington, *Data Reduction and Error Analysis for the Physical Sciences*, McGraw-Hill, New York, 1969.
37 P. Hildebrandt and M. Stockburger, *J. Phys. Chem., 88* (1984) 5935.
38 N. Mataga and K. Nishimoto, *Z. Phys. Chem. NF, 13* (1957) 140; FORTRAN program for MS-DOS.
39 R. Hoffmann, *J. Chem. Phys., 39* (1963) 1397; QCPE Program # 344, modified version for MS-DOS.
40 R. S. Mulliken, *J. Chem. Phys., 23* (1955) 1833.
41 H. Baba, L. Goodman and P. C. Valenti, *J. Am. Chem. Soc., 88* (1966) 5410.
42 J. A. Warren, E. R. Bernstein and J. I. Seeman, *J. Chem. Phys., 88* (1988) 871.
43 E. M. Gibson, A. C. Jones, A. G. Taylor, W. G. Bouwman, D. Philips and J. Sandell, *J. Phys. Chem., 92* (1988) 5449.
44 P. C. M. Weissenborn, A. H. Huizer and C. A. G. O. Varma, *Chem. Phys., 126* (1988) 425.